

Intrinsic vortex pinning in superconducting quasicrystals

Yuki Nagai ^{*}

CCSE, Japan Atomic Energy Agency, 178-4-4, Wakashiba, Kashiwa, Chiba 277-0871, Japan

and Mathematical Science Team, RIKEN Center for Advanced Intelligence Project (AIP), 1-4-1 Nihonbashi, Chuo-ku, Tokyo 103-0027, Japan



(Received 28 November 2021; revised 5 May 2022; accepted 27 June 2022; published 16 August 2022)

We numerically show that a vortex pinning occurs in a superconducting quasicrystal without impurities and defects. This vortex pinning is intrinsic since the superconducting order parameter in quasicrystals is always inhomogeneous due to the lack of the translational symmetry. We propose that experiments influenced by vortex pinning effects can detect the atomic-scale inhomogeneous superconducting order parameter in quasicrystals. We develop a numerical method to solve the Bogoliubov-de Gennes equations and gap equations in large systems, which is based on the localized-Krylov subspace and a sparse modeling technique. Two two-dimensional quasicrystals, the Penrose and Amman-Beenker tiling, are considered.

DOI: [10.1103/PhysRevB.106.064506](https://doi.org/10.1103/PhysRevB.106.064506)

I. INTRODUCTION

A quasicrystal has no translational symmetry. Recently, Kamiya *et al.* found that a superconducting phase appears in Al-Zn-Mg quasicrystalline alloys [1]. In superconducting quasicrystals, the Cooper pairs with momentum k and $-k$, which appeared in the conventional picture of the superconductivity, cannot be applied, since momentum is not a good quantum number. The lack of translational symmetry induces an intrinsic atomic-scale inhomogeneous superconducting order parameter in superconducting quasicrystals [2,3].

The detection of the inhomogeneous phenomena in superconducting quasicrystals in experiments is one of the most important pieces of evidence of the existence of exotic superconductivity in quasicrystals. However, there is no experiment that can directly detect a superconducting order parameter in real space. Some theoretical papers found that the local density of states (LDOS), which can be observed by the scanning tunneling microscopy/spectroscopy (STM/STS), has only weak spatial dependence of the spectral gap [2,4], even if the superconducting order parameter fluctuates in atomic scales.

A vortex in superconductors can be directly observed by STS/STS or SQUID experiments. A vortex has been used to study superconducting properties, since bound states around a vortex reflect the information of the superconducting order parameter and the electronic structure. For example, a vortex in NbSe₂ has a sixfold star-shaped LDOS originating from a sixfold anisotropic superconducting pairing symmetry [5,6]. Recently, Fermi surface anisotropy in conventional superconductor lanthanum has been detected by the STM/STS [7].

With the use of a vortex in superconducting quasicrystals, we propose that the inhomogeneous superconducting state in quasicrystals can be detected. We focus on the fact that the energy level of the minimum vortex bound states depends

on how the superconducting order parameter is suppressed around a vortex since a region where the order parameter becomes small around a vortex can be regarded as a region inside a quantum well for quasiparticles. In general, the energy level becomes small if the size of the suppressed region is large (i.e., inside a large quantum well). In addition, the size of the suppressed region depends on the amplitude of the superconducting order parameter. Therefore, since the amplitude of the order parameter changes in superconducting quasicrystals in real space, the energy level of the vortex bound states should depend on the position of the vortex.

In this paper, we show an intrinsic vortex pinning due to a strong inhomogeneous superconducting order parameter in superconducting quasicrystal, which can be detected experimentally. A vortex moves to find a position where the free energy becomes minimum. In other words, vortices are pinned even if there is no impurity or defect. To make this statement general, we consider two kinds of superconducting quasicrystals, superconducting tight-binding models with Penrose and Ammann-Beenker (AB) tiling. A numerical technique is proposed for solving the Bogoliubov-de Gennes equations in a large inhomogeneous tight-binding model, which is based on the localized-Krylov subspace and sparse modeling (SpM) techniques [4].

This paper is organized as follows. In Sec. II, we show the model and method that we consider. We show the theoretical model Hamiltonian of the two-dimensional tight-binding Bardeen-Cooper-Schrieffer (BCS) Hamiltonian on the Penrose and AB tiling. We propose a numerical approach for large-scale superconductors, a localized-Krylov reduced shifted conjugate gradient method with sparse modeling (LK-RSCG with SpM), which is based on the LK subspace and SpM techniques. We introduce the dual-grid method to construct models for quasicrystals, which is based on a projection from a high-dimensional lattice. With the use of this method, one can easily generate different patterns of tiling. In Sec. III, we show the numerical results that the intrinsic vortex pinning occurs in superconducting quasicrystals. In Sec. IV, we

*nagai.yuki@jaea.go.jp

discuss the mechanism of the intrinsic vortex pinning and its position. In Sec. V, the summary is given.

II. MODEL AND METHOD

A. Hamiltonian

We consider the tight-binding BCS Hamiltonian on the Penrose and AB tiling given as

$$\mathcal{H} = \sum_{ij,\sigma} (-t_{ij} - \mu\delta_{ij}) c_{i\sigma}^\dagger c_{j\sigma} + \sum_i [\Delta_i c_{i\uparrow}^\dagger c_{i\downarrow}^\dagger + \text{H.c.}], \quad (1)$$

where $c_{i\sigma}^\dagger$ creates the electron with spin σ at site i and μ denotes the chemical potential. t_{ij} is the transfer integral which connects a bond on the tiling. We consider that the intensity of the hopping is uniform $t_{ij} = t$ on bonds. For simplicity, we consider on-site s -wave superconductivity. We use the unit system with $\hbar = k_B = 1$. One can diagonalize \mathcal{H} to solve the BdG equations expressed as

$$\sum_j \hat{H}_{i,j} \begin{pmatrix} u_\gamma(\mathbf{r}_j) \\ v_\gamma(\mathbf{r}_j) \end{pmatrix} = E_\gamma \begin{pmatrix} u_\gamma(\mathbf{r}_i) \\ v_\gamma(\mathbf{r}_i) \end{pmatrix}, \quad (2)$$

where the $2N \times 2N$ Hamiltonian matrix \hat{H} is defined as

$$\hat{H}_{i,j} = \begin{pmatrix} [\hat{H}^N]_{ij} & \Delta_i \delta_{ij} \\ \Delta_i^* \delta_{ij} & -[\hat{H}^{N*}]_{ij} \end{pmatrix}. \quad (3)$$

Here $[\hat{H}^N]_{ij} = -t_{ij} - \mu\delta_{ij}$ and N is the number of the lattice sites. The s -wave superconducting order parameter is defined as

$$\Delta_i = U \langle c_{i\downarrow} c_{i\uparrow} \rangle, \quad (4)$$

where Δ_i is the superconducting order parameter at a site i and U is the on-site pairing interaction. In this paper, Δ_i is calculated self-consistently. In Eq. (4), we assume that the on-site pairing interaction does not depend on the lattice site. Although it seems more reasonable that the interaction has the lattice-site dependence, the strong inhomogeneity of the superconducting order parameter has been reported in both Penrose and AB quasicrystals with site-independent pairing interactions [2,8]. In the mean-field level, the physical properties of the systems are directly determined by the mean fields, not the interactions. Phenomena induced by the site-dependent pairing interaction in the disordered Hubbard model are out of scope in this paper.

B. Construction of quasicrystals: Dual-grid method

We introduce the dual-grid method to construct models for quasicrystals [9,10]. In this paper, we consider the Penrose quasicrystal and AB quasicrystal, which are famous two-dimensional quasicrystals. There are several methods to construct models for quasicrystals. In last five years, the inflation-deflation method [11] has been used to treat a large size cluster [2–4,12–17]. In the inflation-deflation method, a quasicrystal is generated by iteratively applying the inflation-deflation rule. Usually, the quasicrystal generated by the inflation-deflation method has a high symmetric point at the center of a lattice. For example, in the Penrose quasicrystal, there is a tenfold rotational symmetry around

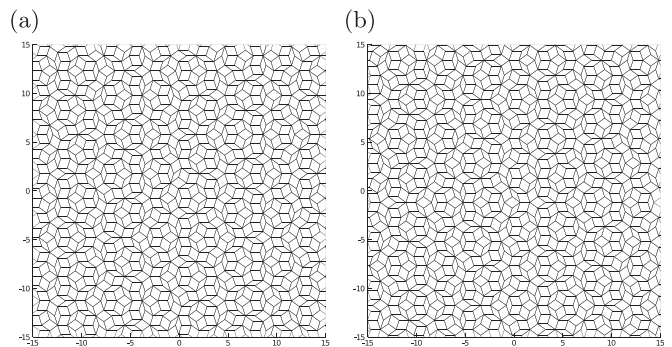


FIG. 1. Penrose lattices obtained by the dual grid method with different $\vec{\gamma}^T$. (a) $\vec{\gamma}^T = (0.1, 0.7, -0.98, 0.43, -\sum_{\mu=0}^3 \gamma_\mu)$ and (b) $\vec{\gamma}^T = (1/7, 1/9, -3/4, -\sqrt{5}, -\sum_{\mu=0}^3 \gamma_\mu)$. The total numbers of lattice sites are 60 831 and 60 863, respectively.

a center. However, in realistic quasicrystals, we cannot assume that a rotational symmetry exists around the center of a system.

We adopt the so-called dual-grid method to generate the quasicrystals. It is known that a D -dimensional quasicrystal can be obtained by the projection of a particularly cut slice of the M -dimensional euclidian hyperlattice onto a D -dimensional plane. As shown in Figs. 1 and 2, we can easily generate different patterns of Penrose or AB lattices with different $\vec{\gamma}$, which determines a position of cut slice of the M -dimensional Euclidian hyperlattice. In other words, one can reproduce same quasicrystal structure with the use of same $\vec{\gamma}$. The detail of the dual-grid method is shown in Appendix A.

C. Numerical approach for large-scale superconductors: LK-RSCG method with sparse modeling approach

To consider superconducting quasicrystals, we have to solve the BdG Eq. (2) in real space with solving the gap equation Eq. (4) self-consistently. It is very hard to diagonalize the BdG Hamiltonian matrix in large quasicrystals, since the computational complexity to diagonalize the Hamiltonian matrix is $O(N^3)$. Recently, we have proposed the localized Krylov-Bogoliubov-de Gennes method (LK-BdG), whose

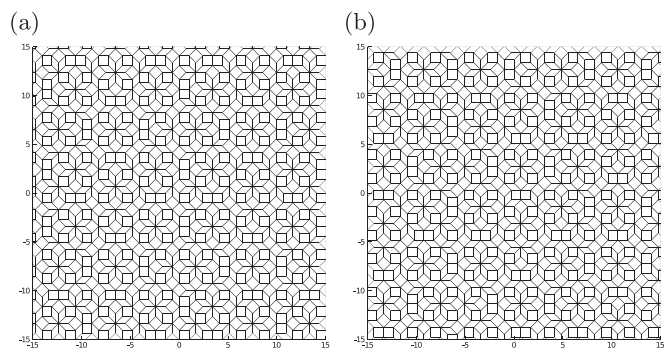


FIG. 2. Ammann-Beenker lattices obtained by the dual grid method with different $\vec{\gamma}^T$. (a) $\vec{\gamma}^T = (0.1, 0.14, -0.23, -\sum_{\mu=0}^2 \gamma_\mu)$ and (b) $\vec{\gamma}^T = (-0.21, 0.29, 0.98, -\sum_{\mu=0}^2 \gamma_\mu)$. The total numbers of lattice sites are 54 579 and 54 607, respectively.

computational complexities are $O(N)$ for self-consistent calculations and $O(1)$ for calculating the local quantities such as the LDOS [4]. In a previous paper, we proposed the Chebyshev polynomial method and the Lanczos method as the applications of the LK-BdG method. In this paper, we adopt the reduced-shifted conjugate-gradient (RSCG) method to control the numerical accuracy [18], which is also one of the applications of LK-BdG method. The RSCG method uses the fact that the mean fields are calculated by the solutions of linear equations as

$$\langle c_{i\downarrow}c_{i\uparrow} \rangle = T \sum_{n=-\infty}^{\infty} \mathbf{e}(i)^T \mathbf{x}(i, \omega_n), \quad (5)$$

where the solutions $\mathbf{x}(i, \omega_n)$ are obtained by solving the following linear equations:

$$(i\omega_n \hat{I} - \hat{H})\mathbf{x}(i, \omega_n) = \mathbf{h}(i). \quad (6)$$

Here, $\omega_n \equiv \pi T(2n+1)$ denotes the fermion Matsubara frequency and $2N$ -component unit-vectors $\mathbf{e}(i)$ and $\mathbf{h}(j)$ ($1 \leq i \leq N$) are defined as

$$[\mathbf{e}(i)]_\gamma = \delta_{i,\gamma}, \quad [\mathbf{h}(i)]_\gamma = \delta_{i+N,\gamma}. \quad (7)$$

Details are shown in Appendix B.

Let us introduce the Localized-Krylov subspace RSCG (LK-RSCG). Equation (6) with different frequencies can be solved simultaneously with the use of the RSCG [18]. Focusing on the fact that the vectors $\mathbf{e}(i)$ and $\mathbf{h}(i)$ are localized in real space, we show that the k th-order Krylov subspace generated by the Hamiltonian matrix given as [4]

$$\mathcal{K}_k(\hat{H}, \mathbf{b}) = \text{span}(\mathbf{b}, \hat{H}\mathbf{b}, \hat{H}^2\mathbf{b}, \dots, \hat{H}^{k-1}\mathbf{b}) \quad (8)$$

is localized in real space. The computational complexity of the matrix-vector products in the RSCG method $O(N)$ is replaced with $O(k^d)$. Here, d is a spatial dimension [4,19]. In the calculation in this paper, the maximum number of k , which depends on the parameters, is usually around 900.

In addition, to reduce the computational complexity, we introduce the recently developed SpM approach for a Green's function [20–24]. The Green's function in Nambu-Gor'kov space can be defined as the solution of the Nambu-Gor'kov equation:

$$(i\omega_n \hat{I} - \hat{H})\hat{G}(i\omega_n) = \hat{1}. \quad (9)$$

With the use of the intermediate representation (IR) basis, the matrix element of the Green's function is written as

$$G_{ij}(i\omega_n) = \sum_{l=0}^{N_{\text{IR}}-1} G_{l,ij} U_l(i\omega_n), \quad (10)$$

where $U_l(i\omega_n)$ is a basis function of the IR basis and N_{IR} is a number of the basis functions (see Appendix B 2). Here, G_{ij} is the element of the matrix-valued Green's function $G_{ij} = [\hat{G}]_{ij}$. The superconducting mean fields are given as

$$\langle c_{i\downarrow}c_{i\uparrow} \rangle = \sum_{l=0}^{N_{\text{IR}}-1} U_l(\beta) \sum_{k=0}^{N_{\text{IR}}-1} [U^{-1}]_{lk} \mathbf{e}(i)^T \mathbf{x}(i, \omega_k). \quad (11)$$

Although the size of N_{IR} depends on a cutoff parameter in the IR basis, N_{IR} is small, around 10–100. With the use of the

TABLE I. Reduction of computational complexity. Here, N , N_{IR} , n_{cut} , m are the matrix size of the Hamiltonian, the number of the intermediate basis, the number of the Matsubara summations, and the number of the iteration steps for the RSCG. $O(N^3)$ in the table is the computational cost for the full diagonalization method of the Hamiltonian matrix.

Methods	Computational complexity
SpM approach	$O(n_{\text{cut}}) \rightarrow O(N_{\text{IR}})$
LK matrix-vector operation	$O(N) \rightarrow O(1)$
Total	$O(N^3) \rightarrow O(mN_{\text{IR}}) + O(Nm)$

RSCG method and IR basis, we can calculate Eq. (5) with high accuracy. With the use of the SpM, the total complexity for self-consistent calculation is $O(mN_{\text{IR}}) + O(Nm)$. The reduction of the computational complexity is summarized in Table I.

III. RESULTS

We solve the gap equations self-consistently in the Penrose and AB quasicrystals. We consider the temperature $T = 10^{-3}t$ and the cutoff frequency $\omega_{\text{max}} = 10t$, where the number of the IR basis N_{IR} is 104.

A. Basic properties of superconducting quasicrystal without vortices

Superconductivity without vortices on the Penrose and AB tiling has been studied by several groups, respectively [8,13]. According to previous studies, there are two important properties of superconductivity on quasicrystals.

The first is a nonuniform distribution of the superconducting order parameter. Even if the on-site pairing interaction does not depend on a position in real space, the superconducting order parameter defined by Eq. (4) is inhomogeneous in real space. As shown in Fig. 3, we confirm that similar inhomogeneity occurs in our parameter set of the Penrose tiling. Here, we consider the chemical potential $\mu = -t$ and the on-site pairing interaction $U = -2t$. We choose $\vec{\gamma}_A = (0.1, 0.7, -0.98, 0.43, -\sum_{\mu=0}^3 \gamma_\mu)$ and the radius of the system is $172a$, where a is the bond length of the lattice and the total number of the lattice sites is 119 026. The upper panel in Fig. 3, the spatial average of the amplitude of order parameter is $\sim 0.24344t$. We also confirm that the spatial average of the amplitude of order parameter does not depend on the parameter γ .

The second is that many thermodynamic properties in superconducting quasicrystals are almost indistinguishable from ones in conventional BCS superconductors. Araújo and Andrade found no evidence of superconductivity islands although the superconducting order parameter is inhomogeneous in AB quasicrystals and they concluded that quasicrystals are prone to display conventional BCS-like superconductivity [8]. Takemori *et al.* calculated the LDOS, specific heat, and I-V characteristics in Penrose quasicrystals [13]. Although they claimed that there are differences between Penrose superconducting quasicrystals and conventional BCS superconductors, the difference is not very large, which might

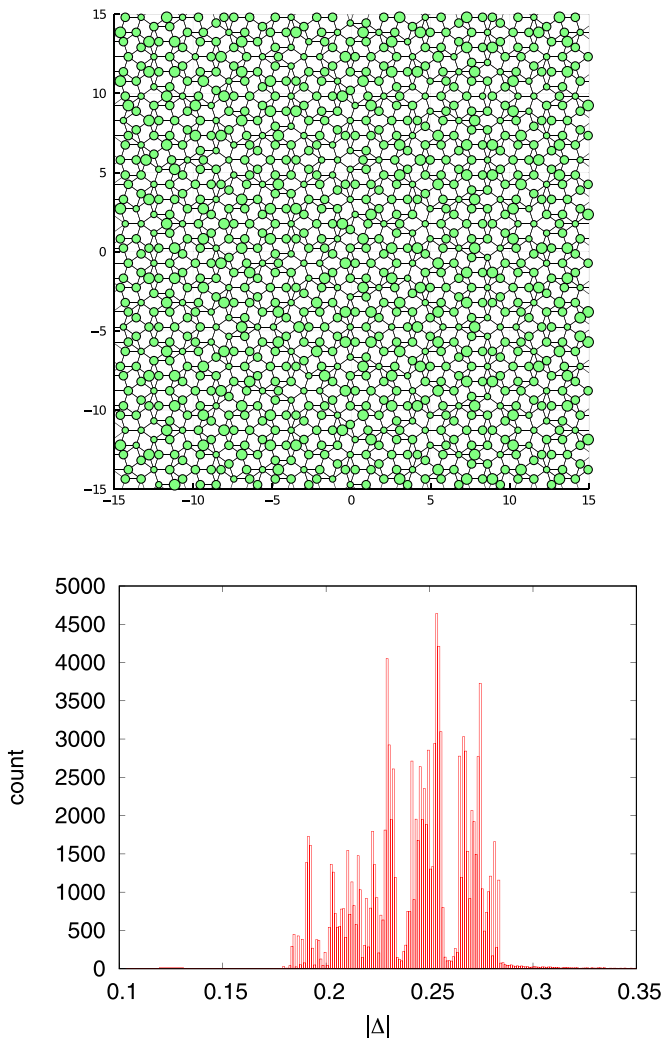


FIG. 3. Upper panel: Superconducting order parameter around the origin in a system characterized by $\vec{\gamma}_A^T = (0.1, 0.7, -0.98, 0.43, -\sum_{\mu=0}^3 \gamma_\mu)$. The size of the circles is proportional to the amplitude of the order parameter. Lower panel: Superconducting order parameter distribution. The unit of the order parameter is the hopping amplitude t .

not be detected in experiments. The spectrum gap in the LDOS is almost uniform in real space where the order parameter is not uniform, which suggests that the STM/STS measurements cannot detect the inhomogeneity of the superconducting order parameter. There is the jump of the specific heat at the critical temperature and the amplitude of the jump ΔC is relatively smaller than the value in conventional BCS theory. However, in real materials, the jump ΔC depends on materials even if the superconductivity is explained by the BCS theory. In addition, according to a previous result on AB quasicrystals [8], the increase of the critical temperature due to a multifractal nature of the electronic state is not found in this system, as is expected on disordered systems close to the Anderson metal-insulator transition.

It is difficult to detect the inhomogeneous phenomena in experiments of superconducting quasicrystals without magnetic fields. Therefore, we need a vortex as a source of the quasiparticle excitation.

B. Electronic structure with a vortex

Let us consider systems with a vortex. We study superconductivity in Penrose and AB quasicrystals in the type-II limit (the magnetic penetration depth $\lambda \rightarrow \infty$). As the initial state, we locate a vortex at a center in each system. After solving the gap equations self-consistently, a vortex moves to find the position where the free energy becomes minimum. We show results about both Penrose and AB lattices in this section.

1. Penrose quasicrystal

We consider four patterns of Penrose lattices, which are determined by the following $\vec{\gamma}$, respectively:

$$\vec{\gamma}_A^T = \left(0.1, 0.7, -0.98, 0.43, -\sum_{\mu=0}^3 \gamma_\mu \right), \quad (12)$$

$$\vec{\gamma}_B^T = \left(1/7, 1/9, -3/4, -\sqrt{5}, -\sum_{\mu=0}^3 \gamma_\mu \right), \quad (13)$$

$$\vec{\gamma}_C^T = \left(0.1, 0.2, 0.3, 0.4, -\sum_{\mu=0}^3 \gamma_\mu \right), \quad (14)$$

$$\vec{\gamma}_D^T = \left(-0.4, -0.13, 2.4, 0.89, -\sum_{\mu=0}^3 \gamma_\mu \right). \quad (15)$$

We consider the chemical potential $\mu = -t$ and the on-site pairing interaction $U = -2t$.

After solving the gap equations self-consistently, a vortex is not located at the center as shown in Fig. 4. The position of the vortex is different in each system but the local lattice structures around a vortex look similar to each other. Since the system with the converged gap distribution has minimum free energy, the free energy depends on the vortex position on the Penrose quasicrystal. Therefore, we claim that the intrinsic vortex pinning occurs on superconducting quasicrystals.

Vortex bound states in superconductors have rich information about a superconducting order parameter. We calculate the low-energy eigenvalues of the BdG Hamiltonian in four systems, originating from the bound states around a vortex core. As shown in Fig. 5, we find that the low-energy eigenvalue distribution does not depend on systems. The lowest eigenvalue is around $0.5E_0$. Here, $E_0 (= 0.243t)$ is the absolute minimum of the eigenvalues in the system without vortex, where the total number of the lattice sites is 119 026. In conventional s -wave BCS superconductors, the energy levels are equally spaced, which is characterized by Δ^2/E_F , a ratio of the order parameter Δ and Fermi energy E_F [6]. However, we found that the energy of the first excited vortex bound state is much larger than the energy difference between the first and second bound states. This quantum-limit behavior might be observed by the STM/STS experiments. The reason for this behavior is explained in the discussion section.

The size of the vortex core in superconducting Penrose lattice looks small in Fig. 4. This small core might be understood by a core shrinkage effect, the so-called Kramer-Pesch effect [6,25], which occurs conventional superconductors. In conventional superconductors, the vortex core is characterized by the coherence length v_F/Δ , where v_F is the Fermi velocity. The Kramer-Pesch effect becomes large when the

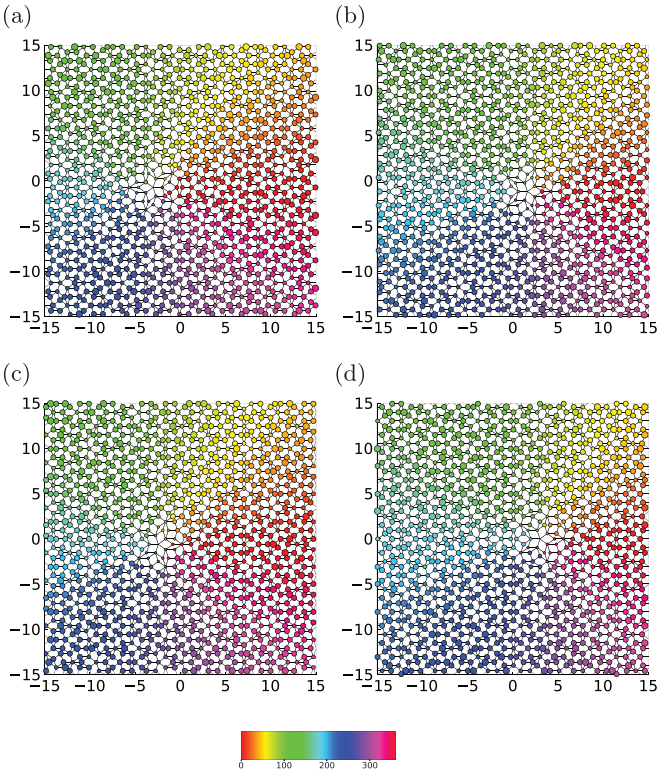


FIG. 4. Superconducting order parameter with different $\vec{\gamma}^T$ in superconducting Penrose quasicrystals. The size of the circles is proportional to the amplitude of the order parameter. The color represents the phase of the order parameter. (a) $\vec{\gamma}_A^T = (0.1, 0.7, -0.98, 0.43, -\sum_{\mu=0}^3 \gamma_\mu)$, (b) $\vec{\gamma}_B^T = (1/7, 1/9, -3/4, -\sqrt{5}, -\sum_{\mu=0}^3 \gamma_\mu)$, (c) $\vec{\gamma}_C^T = (0.1, 0.2, 0.3, 0.4, -\sum_{\mu=0}^3 \gamma_\mu)$, and (d) $\vec{\gamma}_D^T = (-0.4, -0.13, 2.4, 0.89, -\sum_{\mu=0}^3 \gamma_\mu)$.

energy-level spacing of the bound states is large [6]. We should note that the coherence length cannot be determined with the use of the Fermi velocity in quasiperiodic systems,

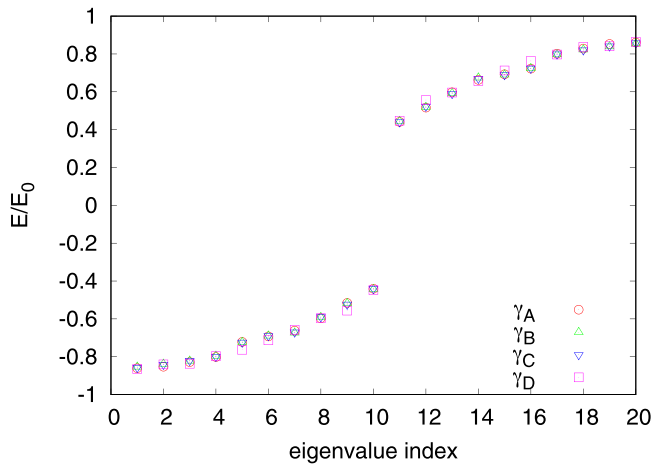


FIG. 5. Eigenvalues in different systems with a vortex in the Penrose quasicrystal. $E_0 = 0.243t$ is the absolute minimum of the eigenvalues in the system without vortex, where the total number of the lattice sites is 119 026.

since the Fermi velocity is not defined in these systems. Therefore, the definition of the coherence length is not clear in superconducting quasicrystals.

We should point out that the energy of the lowest vortex bound states is much larger than the bound energy in the system created by the inflation-deflation method in our previous paper [4]. We have reported that the energy of the vortex bound states is almost zero in the system [4]. This difference comes from the position of the vortex. In the previous paper, the vortex cannot move from a center because the vortex is located at a center of the system with a tenfold symmetry. The minimum energy is determined by the local structure around a center. In 21 106-site and 143 806-site Penrose lattice systems whose local lattice structure around a center is the same, the minimum energy is close to zero. However, we have also reported that, in the 375 971-site Penrose lattice whose local structure differs from that in the 21 106 site, the minimum energy level in a vortex core is larger. On the other hand, in systems created by the dual-grid method in this paper, the vortex can move since there is no local tenfold symmetry. These results suggest that the free energy depends on the local lattice structure around a vortex, which is discussed later.

2. Ammann-Beenker quasicrystal

We consider the AB quasicrystal to confirm whether an intrinsic vortex pinning occurs in another quasicrystal structures. We consider two patterns of AB lattices, which are determined by the following $\vec{\gamma}$, respectively:

$$\vec{\gamma}_A^T = \left(0.1, 0.14, -0.23, -\sum_{\mu=0}^2 \gamma_\mu \right), \quad (16)$$

$$\vec{\gamma}_B^T = \left(-0.21, 0.29, 0.98, -\sum_{\mu=0}^2 \gamma_\mu \right). \quad (17)$$

In the system without a vortex in our parameter set, the mean value of the superconducting order parameter is $0.26593t$. The basic property of the superconducting AB quasicrystal is similar to the Penrose one. We note that there is a paper discussing the system without a vortex [8]. For systems with a vortex, we initially put a vortex at a center and solve the gap equations. After solving gap equations self-consistently, a vortex is not located at the center as shown in Fig. 6. We find that the local lattice structures near a vortex in two systems are similar to each other. We also calculate the low-energy eigenvalues of two systems as shown in Fig. 7. One can clearly find that the bound-state energy of a vortex is the same in two systems. Therefore, the vortex in the AB lattice is also pinned.

IV. DISCUSSIONS

A. Mechanism of the intrinsic vortex pinning in superconducting quasicrystals

We found that the intrinsic vortex pinning occurs in superconducting quasicrystals. In the mean-field level, solving the gap Eq. (4) means finding the distribution of the superconducting order parameter where the thermodynamic potential becomes minimum. The vortex in superconducting Penrose and AB tight-binding models is pinned, where the energies

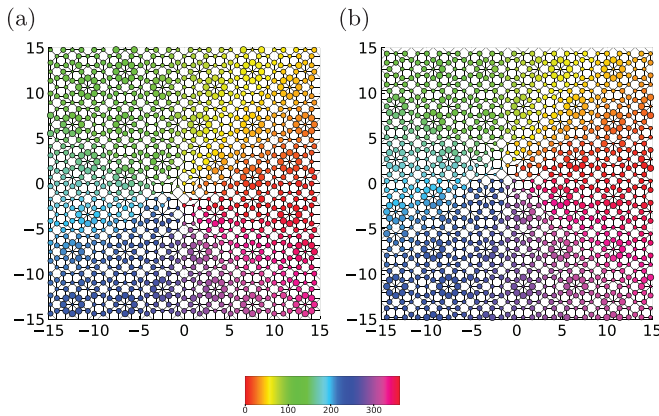


FIG. 6. Superconducting order parameter with different $\bar{\gamma}^T$ in superconducting Ammann-Beenker quasicrystals. The size of the circles is proportional to the amplitude of the order parameter. The color represents the phase of the order parameter. (a): $\bar{\gamma}^T = (0.1, 0.14, -0.23, -\sum_{\mu=0}^2 \gamma_{\mu})$ and (b): $\bar{\gamma}^T = (-0.21, 0.29, 0.98, -\sum_{\mu=0}^2 \gamma_{\mu})$. The mean value of the order parameter in the system without a vortex is 0.26593*t*.

of vortex bound states are large. We explain the reason as follows. We calculate the low-energy eigenvalues of the BdG Hamiltonian in four systems, which reflects the bound states around a vortex core. As shown in Fig. 5, we find that the low-energy eigenvalue distribution does not depend on systems, which suggests that a vortex is pinned where a thermodynamic potential becomes minimum. The thermodynamic potential Ω in the BdG framework is defined as [26–28]

$$\Omega = -T \sum_{\gamma=1}^{2N} \ln \left[1 + \exp \left(\frac{E_{\gamma}}{T} \right) \right] - \sum_i \frac{|\Delta_i|^2}{U}. \quad (18)$$

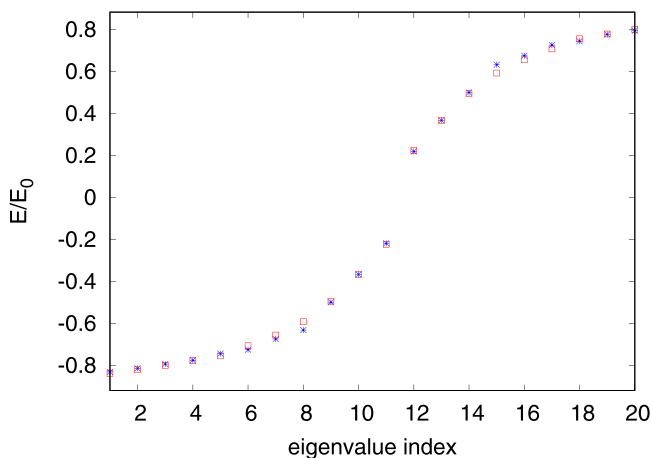


FIG. 7. Eigenvalues in different systems with a vortex in Ammann-Beenker lattices. $E_0 = 0.2597t$ is the absolute minimum of the eigenvalues in the system without vortex, where the total number of the lattice sites is 54 604.

Since the temperature is very low ($T = 10^{-3}t$), Ω is expressed as [28]

$$\Omega \sim - \sum_{\gamma=1}^{2N} E_{\gamma} \theta(E_{\gamma}) - \sum_i \frac{|\Delta_i|^2}{U}, \quad (19)$$

which is equivalent to the internal energy. Here $\theta(x)$ is the Heaviside step function. The first term in Eq. (19) decreases when the bound-state energy becomes larger. The second term is usually small since the system satisfies the relation $|\Delta_i|^2/|U| < E_0$. Here, E_0 is the absolute minimum of the eigenvalues in the system without vortex. As shown in Eq. (19), the lower energy bound state contributes less to the internal energy. In our previous paper [4], we showed the minimum of the bound states depends on the local lattice structure around a vortex center in the Penrose quasicrystals. Therefore, a vortex moves during self-consistent iteration loops and is pinned at the position where the total energy becomes minimum on superconducting quasicrystals.

We try to estimate the energy change by changing the position of a vortex. We should note that, in self-consistent calculations, a vortex moves to find a local energy minima so we cannot evaluate the vortex-position dependent energy. However, we can roughly estimate the energy difference between two vortex configurations by focusing on the bound-state energy. By assuming that the superconducting order parameter distribution far from a vortex is the same between these two vortex configurations, the difference of the total energy is determined by the difference of the bound-state energy. In Fig. 5, the lowest bound-state energy is around $0.5E_0$, while, in Ref. [4], the lowest bound-state energy is zero. Therefore, the energy scale by changing the position of a vortex is about E_0 .

We claim that this intrinsic vortex pinning occurs in three-dimensional realistic materials, since the vortex pinning originates from the inhomogeneous superconducting order parameter. In general, the superconducting order parameter is defined as $\Delta(\mathbf{R}, \mathbf{r})$, where \mathbf{R} and \mathbf{r} are the center-of-mass and the relative coordinates, respectively. In superconductors with translational symmetry, the superconducting order parameter becomes $\Delta(\mathbf{R}, \mathbf{r}) = \Delta(\mathbf{r})$. In quasicrystals, there is no translational symmetry. The Cooper pairs in quasicrystals cannot be characterized by single momenta. Then, Fourier-transformed order parameter $\Delta(\mathbf{k}_1, \mathbf{k}_2)$ becomes complicated function in momentum space [2]. In real space, there should be the center-of-mass dependence $\Delta(\mathbf{R}, \mathbf{r})$. Therefore, the inhomogeneous superconducting order parameter is the intrinsic effect in superconducting quasicrystal in any dimension.

B. Position of vortices on superconducting quasicrystals

A Penrose lattice has eight types of vertices with the nomenclature of de Bruijn [9,10,17]. In our parameter set of the Penrose superconductors, as shown in Fig. 4, the vortex is pinned at the S5 vertex, which has a local fivefold rotational symmetry. We also confirm that vortices are pinned at these vertices even if there are several vortices in these systems. In a system without a vortex, the superconducting order parameter becomes minimum at this S5 vertex and becomes large at the other fivefold-symmetric vertex, the so-called S vertex,

as shown in Fig. 3. We have studied the electronic structure in the system where the vortex is located at S vertex in our previous paper [4]. As shown in Fig. 2(d) in Ref. [4], the vortex has near-zero energy bound states. Since near-zero bound states contribute less to the thermodynamic potential given as Eq. (19), the vortex is not pinned at the S vertex. According to a paper by Sakai *et al.* [29], S and S5 vertices constitute the superlattice as shown in Fig. 9 in Ref. [29]. Since the vortex is pinned at S5 vertex not at the S vertex, a vortex lattice does not constitute a Penrose-like superlattice in systems with our parameter set.

Vortex lattice structures become unique in superconducting quasicrystals, although we do not confirm that a vortex is always pinned at the S5 vertex in all parameter regions of the Penrose superconducting tight-binding model. The important point is that the amplitude of the superconducting order parameter depends on the local lattice structure of the quasicrystals without magnetic fields. Our calculation suggests that the site that has a relatively smaller gap amplitude can be a pinning site. Since the vortex suppresses the superconducting order parameter around a center of the vortex, it might be better to make the amount of the suppression small in terms of the total minimization of the thermodynamic potential.

We should note that the vortex lattice structure is determined not only by the pinning site distributions but also by the interaction between vortices [30]. In a conventional superconductor, vortices form the Abrikosov triangular lattice. What kind of vortex structure occurs on quasicrystalline pinning potentials depends on a cooperation or competition between the pinning potential and vortex-vortex interactions [31,32]. For example, the critical current on systems' quasiperiodic pinning arrays is discussed [31]. A pattern formed by interacting particles on a quasiperiodic potential has also been studied in colloids [33–35]. For example, Archimedian-like ordering is discussed, which occurs as a compromise between the quasicrystalline ordering and triangular ordering [33,35]. A phason dynamics of vortices might be interesting in vortex systems, which has been discussed in colloids [36,37]. Here, the phason is a characteristic behavior in quasiperiodic systems.

C. Experiments to detect vortex pinning

Since STM/STS measurements have atomic-scale resolution, STM/STS can observe the position of a vortex. Therefore, STM/STS measurements can give direct evidence of the inhomogeneous superconductivity in quasicrystals. Since the SQUID measurements also detect the position of a vortex, this also gives concrete evidence. Other experiments influenced by a pinning effect also become tools to detect this inhomogeneity of superconductivity. For example, the critical current should depend on the pinning effect [31].

We consider clean and perfect quasicrystals in this paper. There can be kinds of extrinsic pinning such as voids and twins in realistic materials. In addition, in quasicrystals, there can be so-called phason strain, which is a characteristic dislocation in quasicrystals [38,39]. This dislocation can also become a source of pinning potential. The actual pinning site is determined by the competition between intrinsic and extrinsic effect.

V. SUMMARY

We showed that an intrinsic vortex pinning due to the inhomogeneous superconducting order parameter occurs in superconducting quasicrystals. We confirmed that the intrinsic vortex pinning occurs in systems with several vortices in both Penrose and AB quasicrystals. We proposed a method to solve BdG equations on large tight-binding models, which is based on the LK subspace and the SpM technique. If STM/STS or SQUID measurements can observe a vortex pinning in clean quasicrystals, this becomes evidence of the inhomogeneous superconductivity in quasicrystals.

ACKNOWLEDGMENTS

Y.N. was partially supported by JSPS-KAKENHI Grants No. 18K11345 and No. 20H05278. The calculations were performed by the supercomputing system HPE SGI8600 at the Japan Atomic Energy Agency.

APPENDIX A: DUAL-GRID METHOD

1. Hyperlattices for quasicrystals

It is known that a D -dimensional quasicrystal can be obtained by the projection of a particularly cut slice of the M -dimensional euclidian hyperlattice onto a D -dimensional plane, which is expressed as

$$\mathbf{r}_{\text{lattice}} = \sum_{\mu=0}^{M-1} K_{\mu} \mathbf{d}_{\mu}, \quad (\text{A1})$$

where $\vec{K} = (K_1, \dots, K_M)$ are the M -dimensional lattice points labeled with integers K_{μ} . In this Appendix, we use \vec{A} as the M -dimensional vector and \mathbf{a} as the D -dimensional vector. In the Penrose (AB) lattice, the hyperlattice is defined in five- (four-) dimensional space. The \vec{d} vectors in the Penrose and AB lattices are, respectively, defined as

$$\mathbf{d}_{\mu}^{\text{Penrose}} = \begin{pmatrix} \cos\left(\frac{2\pi\mu}{5}\right) \\ \sin\left(\frac{2\pi\mu}{5}\right) \end{pmatrix}, \quad (\text{A2})$$

$$\mathbf{d}_{\mu}^{\text{AB}} = \begin{pmatrix} \cos\left(\frac{\pi\mu}{4}\right) \\ \sin\left(\frac{\pi\mu}{4}\right) \end{pmatrix}. \quad (\text{A3})$$

We consider an M -dimensional vector \vec{R} on a two-dimensional plane in M -dimensional space defined as

$$\vec{R} = x\vec{D}_1 + y\vec{D}_2 + \vec{\gamma}, \quad (\text{A4})$$

where $\mathbf{r}^T = (x, y)$ is a coordinate on the two-dimensional plane and $\vec{\gamma}^T = (\gamma_0, \gamma_1, \gamma_2, \gamma_3, \gamma_4)$ ($\sum_{\mu} \gamma_{\mu} = 0$) consists of M real numbers representing the shift in M dimensions. Here, the M -dimensional vector \vec{D}_i is defined as

$$\vec{D}_m^T = ([\mathbf{d}_0]_m, \dots, [\mathbf{d}_{M-1}]_m). \quad (\text{A5})$$

For example, in the Penrose tiling, we have

$$\vec{D}_1^T = [1, \cos(\theta), \cos(2\theta), \cos(3\theta), \cos(4\theta)], \quad (\text{A6})$$

$$\vec{D}_2^T = [0, \sin(\theta), \sin(2\theta), \sin(3\theta), \sin(4\theta)], \quad (\text{A7})$$

with $\theta \equiv 2\pi/5$. If we can find the hyperlattice point \vec{K} close to the two-dimensional plane defined in Eq. (A4), the

corresponding two-dimensional real space point $\mathbf{r}_{\text{lattice}}$ becomes a vertex of a tiling.

2. Dual grids

To find the hyperlattice point \vec{K} close to the two-dimensional plane, we consider the points where the cross sections of two grid lines α and β are on the two-dimensional plane in M -dimensional space, expressed as

$$K_\alpha = \mathbf{d}_\alpha^T \mathbf{r} + \gamma_\alpha, \quad (\text{A8})$$

$$K_\beta = \mathbf{d}_\beta^T \mathbf{r} + \gamma_\beta, \quad (\text{A9})$$

where K_α and K_β are two integers. With the use of the vector \mathbf{r} , the hyperlattice point \vec{K} can be obtained by

$$K_\alpha = \lceil \mathbf{d}_\alpha^T \mathbf{r} + \gamma_\alpha \rceil. \quad (\text{A10})$$

We can easily generate different patterns of Penrose or AB lattices with different $\vec{\gamma}$, as shown in Figs. 1 and 2. In other words, one can reproduce same quasicrystal structures with the use of same $\vec{\gamma}$.

APPENDIX B: DETAILS OF NUMERICAL APPROACH FOR LARGE-SCALE SUPERCONDUCTORS

1. Local density of states and mean-fields

Without diagonalizing the BdG Hamiltonian directly, we can calculate physical observable and mean fields with the use of the one-particle Green's function defined as

$$\hat{G}(\tau) = -\langle T_\tau \boldsymbol{\psi}(\tau) \boldsymbol{\psi}(0)^\dagger \rangle, \quad (\text{B1})$$

where τ is imaginary time. Here, a $2N$ component creation operator in the Nambu space $\boldsymbol{\psi}^\dagger$ is defined as $\boldsymbol{\psi}^\dagger \equiv (c_{1\uparrow}^\dagger, \dots, c_{N\uparrow}^\dagger, c_{1\downarrow}, \dots, c_{N\downarrow})$ for a spin-singlet single-band superconductivity with N lattice sites. The one-particle Green's function in complex energy plane z is calculated as

$$\hat{G}(z) = (z\hat{I} - \hat{H})^{-1}. \quad (\text{B2})$$

For example, the LDOS with a quantum index i (e.g., a site index or spin-index, etc.) and the mean field $\langle c_{i\downarrow} c_{i\uparrow} \rangle$ are, respectively, expressed as

$$N(\omega, i) = -\frac{1}{2\pi i} \mathbf{e}(i)^T \hat{d}(\omega) \mathbf{e}(i), \quad (\text{B3})$$

$$\langle c_{i\downarrow} c_{i\uparrow} \rangle = \frac{1}{2\pi} \int_{-\infty}^{\infty} d\omega \mathbf{e}(i)^T \hat{d}(\omega) \mathbf{h}(i), \quad (\text{B4})$$

where the difference of the retarded and advanced Green's function matrices $\hat{d}(\omega)$ is determined as $\hat{d}(\omega) = \hat{G}^R(\omega) - \hat{G}^A(\omega)$. Here, we introduce the following $2N$ -component unit vectors $\mathbf{e}(i)$ and $\mathbf{h}(j)$ ($1 \leq i \leq N$), which are, respectively, defined as

$$[\mathbf{e}(i)]_\gamma = \delta_{i,\gamma}, \quad [\mathbf{h}(i)]_\gamma = \delta_{i+N,\gamma}. \quad (\text{B5})$$

The mean fields are also expressed with the Matsubara Green's function as [18]

$$\langle c_{i\downarrow} c_{i\uparrow} \rangle = T \sum_{n=-\infty}^{\infty} \mathbf{e}(i)^T \hat{G}(i\omega_n) \mathbf{h}(i). \quad (\text{B6})$$

The $2N \times 2N$ matrix $\hat{G}(i\omega_n)$ is the Green's function with the Fermion Matsubara frequency $\omega_n \equiv \pi T(2n+1)$ defined as

$$\hat{G}(i\omega_n) \equiv [i\omega_n \hat{I} - \hat{H}]^{-1}. \quad (\text{B7})$$

By solving the linear equations defined as

$$(i\omega_n \hat{I} - \hat{H}) \mathbf{x}(i, \omega_n) = \mathbf{h}(i), \quad (\text{B8})$$

the superconducting mean fields are expressed as

$$\langle c_{i\downarrow} c_{i\uparrow} \rangle = T \sum_{n=-\infty}^{\infty} \mathbf{e}(i)^T \mathbf{x}(i, \omega_n). \quad (\text{B9})$$

By solving Eqs. (4) and (B9) self-consistently, we obtain the superconducting ground states of quasicrystals. Usually, one introduces a cutoff Matsubara frequency $\omega_{n\text{cut}}$ to approximate the above summation, where the number of the Matsubara frequencies becomes finite. We have introduced the RSCG method [18], which solves Eq. (B9) with different frequencies simultaneously. We should note that the computational complexity based on this Matsubara formalism increases with decreasing temperature since the number of the Matsubara frequencies increases with fixing a cutoff $\omega_{n\text{cut}}$. The complexity for calculating a mean field at site i is estimated as $O(mn_{\text{cut}}) + O(2Nm)$, where the first term originates from the Matsubara summation and the second term originates from a sparse-matrix vector operation. Here, m is the number of the iteration steps for the RSCG. The total complexity for self-consistent calculation is $O(mNn_{\text{cut}}) + O(2N^2m)$, since we have to calculate the mean fields everywhere.

2. Sparse modeling approach: Intermediate representation for Green's functions

There is another method so-called SpM approach [20–24] to make the infinity Matsubara summation in Eq. (5) computable. In SpM, the intermediate IR basis is introduced to express information of the Green's function. The IR basis originates from the Lehmann representation of the single-particle Green's function

$$G_{AB}(\tau) = -\int_{-\omega_{\text{max}}}^{\omega_{\text{max}}} d\omega K(\tau, \omega) \rho_{AB}(\omega), \quad (\text{B10})$$

where $G_{AB}(\tau)$ is defined as

$$G_{AB}(\tau) = -\langle T_\tau A(\tau) B(0) \rangle. \quad (\text{B11})$$

The operators A and B should be one of creation or annihilation operators. The kernel $K(\tau, \omega)$ is defined as

$$K(\tau, \omega) \equiv \frac{e^{-\tau\omega}}{1 + e^{-\beta\omega}}, \quad (\text{B12})$$

for $\tau \in [0, \beta]$. The spectrum $\rho_{AB}(\omega)$ is defined as

$$\rho_{AB}(\omega) = -\frac{1}{2\pi i} \lim_{\eta \rightarrow 0^+} (G_{AB}(\omega + i\eta) - G_{AB}(\omega - i\eta)). \quad (\text{B13})$$

Here, the spectrum is bounded in the interval $[-\omega_{\text{max}}, \omega_{\text{max}}]$ (ω_{max} is a cutoff frequency). The IR basis functions are defined through the singular value decomposition (SVD) expressed as

$$K(\tau, \omega) = \sum_l S_l U_l(\tau) V_l(\omega), \quad (\text{B14})$$

where the singular values S_l decays exponentially with increasing l .

The matrix element of the Green's function G_{ij} can be expanded into a compact representation in terms of N_{IR} basis functions, such that in imaginary time and Matsubara frequencies,

$$G_{ij}(\tau) = \sum_{l=0}^{N_{\text{IR}}-1} G_{l,ij} U_l(\tau), \quad (\text{B15})$$

$$G_{ij}(i\omega_n) = \sum_{l=0}^{N_{\text{IR}}-1} G_{l,ij} U_l(i\omega_n), \quad (\text{B16})$$

$$U_l(i\omega_n) = \int_0^\beta d\tau U_l(\tau) e^{i\omega_n \tau}, \quad (\text{B17})$$

where $G_{l,ij}$ are expansion coefficients and $U_l(\tau)$ is the IR basis [20]. The superconducting mean-fields are expressed as

$$\langle c_{i\downarrow} c_{i\uparrow} \rangle = \mathbf{e}(i)^T \hat{G}(\tau = \beta) \mathbf{h}(i) = \sum_{l=0}^{N_{\text{IR}}-1} U_l(\beta) \mathbf{e}(i)^T \hat{G}_l \mathbf{h}(i). \quad (\text{B18})$$

According to Ref. [23], if the sampling points are chosen in the distribution of the roots of the IR basis functions, there

is a useful transformation given as

$$G_l = \sum_{k=0}^{N_{\text{IR}}-1} [\mathbf{U}^{-1}]_{lk} G(i\omega_k), \quad (\text{B19})$$

where \mathbf{U} is a $N_{\text{IR}} \times N_{\text{IR}}$ matrix expressed as

$$[\mathbf{U}]_{lk} = U_l(i\omega_k). \quad (\text{B20})$$

The sampling points ω_k are obtained by the open-source software IRBASIS [20]. Finally, the superconducting mean fields are given as

$$\langle c_{i\downarrow} c_{i\uparrow} \rangle = \sum_{l=0}^{N_{\text{IR}}-1} U_l(\beta) \sum_{k=0}^{N_{\text{IR}}-1} [\mathbf{U}^{-1}]_{lk} \mathbf{e}(i)^T \mathbf{x}(i, \omega_k). \quad (\text{B21})$$

Although the size of N_{IR} depends on a cutoff parameter in the IR basis, N_{IR} is small, around 10–100. With the use of the RSCG method and IR basis, we can calculate Eq. (5) with high accuracy. The computational complexity for the Matsubara summations in the RSCG method $O(mn_{\text{cut}})$ is replaced with $O(mN_{\text{IR}})$.

-
- [1] K. Kamiya, T. Takeuchi, N. Kabeya, N. Wada, T. Ishimasa, A. Ochiai, K. Deguchi, K. Imura, and N. K. Sato, *Nat. Commun.* **9**, 154 (2018).
- [2] S. Sakai, N. Takemori, A. Koga, and R. Arita, *Phys. Rev. B* **95**, 024509 (2017).
- [3] S. Sakai and R. Arita, *Phys. Rev. Research* **1**, 022002(R) (2019).
- [4] Y. Nagai, *J. Phys. Soc. Jpn.* **89**, 074703 (2020).
- [5] H. F. Hess, R. B. Robinson, R. C. Dynes, J. M. Valles, and J. V. Waszczak, *Phys. Rev. Lett.* **62**, 214 (1989).
- [6] N. Hayashi, M. Ichioka, and K. Machida, *Phys. Rev. Lett.* **77**, 4074 (1996).
- [7] H. Kim, Y. Nagai, L. Rózsa, D. Schreyer, and R. Wiesendanger, *Appl. Phys. Rev.* **8**, 031417 (2021).
- [8] R. N. Araújo and E. C. Andrade, *Phys. Rev. B* **100**, 014510 (2019).
- [9] N. de Bruijn, *Indagationes Mathematicae (Proceedings)* **84**, 39 (1981).
- [10] N. de Bruijn, *Indag. Math. (Proceedings)* **84**, 53 (1981).
- [11] D. Levine and P. J. Steinhardt, *Phys. Rev. Lett.* **53**, 2477 (1984).
- [12] A. Koga, *Phys. Rev. B* **102**, 115125 (2020).
- [13] N. Takemori, R. Arita, and S. Sakai, *Phys. Rev. B* **102**, 115108 (2020).
- [14] N. Macé, A. Jagannathan, P. Kalugin, R. Mosseri, and F. Piéchon, *Phys. Rev. B* **96**, 045138 (2017).
- [15] R. Chen, C.-Z. Chen, J.-H. Gao, B. Zhou, and D.-H. Xu, *Phys. Rev. Lett.* **124**, 036803 (2020).
- [16] R. Ghadimi, T. Sugimoto, K. Tanaka, and T. Tohyama, *Phys. Rev. B* **104**, 144511 (2021).
- [17] A. Koga and H. Tsunetsugu, *Phys. Rev. B* **96**, 214402 (2017).
- [18] Y. Nagai, Y. Shinohara, Y. Futamura, and T. Sakurai, *J. Phys. Soc. Jpn.* **86**, 014708 (2017).
- [19] N. Furukawa and Y. Motome, *J. Phys. Soc. Jpn.* **73**, 1482 (2004).
- [20] N. Chikano, K. Yoshimi, J. Otsuki, and H. Shinaoka, *Comput. Phys. Commun.* **240**, 181 (2019).
- [21] Y. Nagai and H. Shinaoka, *J. Phys. Soc. Jpn.* **88**, 064004 (2019).
- [22] J. Otsuki, M. Ohzeki, H. Shinaoka, and K. Yoshimi, *J. Phys. Soc. Jpn.* **89**, 012001 (2020).
- [23] J. Li, M. Wallerberger, N. Chikano, C.-N. Yeh, E. Gull, and H. Shinaoka, *Phys. Rev. B* **101**, 035144 (2020).
- [24] T. Wang, T. Nomoto, Y. Nomura, H. Shinaoka, J. Otsuki, T. Koretsune, and R. Arita, *Phys. Rev. B* **102**, 134503 (2020).
- [25] L. Kramer and W. Pesch, *Z. Phys.* **269**, 59 (1974).
- [26] I. Kosztin, i. c. v. Kos, M. Stone, and A. J. Leggett, *Phys. Rev. B* **58**, 9365 (1998).
- [27] M. V. Hosseini, *Europhys. Lett.* **110**, 47010 (2015).
- [28] Y. Nagai, Y. Ota, and K. Tanaka, *Phys. Rev. B* **96**, 060503(R) (2017).
- [29] S. Sakai, R. Arita, and T. Ohtsuki, *Phys. Rev. B* **105**, 054202 (2022).
- [30] C. Reichhardt and C. J. O. Reichhardt, *Rep. Prog. Phys.* **80**, 026501 (2017).
- [31] V. Misko, S. Savel'ev, and F. Nori, *Phys. Rev. Lett.* **95**, 177007 (2005).
- [32] C. Reichhardt and C. J. Olson Reichhardt, *Phys. Rev. Lett.* **106**, 060603 (2011).
- [33] J. Mikhael, J. Roth, L. Helden, and C. Bechinger, *Nature (London)* **454**, 501 (2008).
- [34] M. Schmiedeberg and H. Stark, *Phys. Rev. Lett.* **101**, 218302 (2008).
- [35] T. Bohlein and C. Bechinger, *Phys. Rev. Lett.* **109**, 058301 (2012).

- [36] J. A. Kromer, M. Schmiedeberg, J. Roth, and H. Stark, [Phys. Rev. Lett.](#) **108**, 218301 (2012).
- [37] J. A. Kromer, M. Schmiedeberg, J. Roth, and H. Stark, [European Phys. J. E](#) **36**, 25 (2013).
- [38] J. E. S. Socolar, [J. Phys. Colloques](#) **47**, C3-217 (1986).
- [39] K. Yamamoto, W. Yang, Y. Nishimura, N. Ikeda, and Y. Matsuo, [MATERIALS TRANSACTIONS](#) **45**, 1255 (2004).